scientific reports

OPEN

Selective isotropic etching of SiO_2 over Si_3N_4 using NF_3/H_2 remote plasma and methanol vapor

Hong Seong Gil[1,4], Doo San Kim[1,4], Yun Jong Jang[1], Dea Whan Kim[3], Hea In Kwon[1], Gyoung Chan Kim[1], Dong Woo Kim[1]✉ & Geun Young Yeom[1,2]✉

In this study, an isotropic etching process of SiO_2 selective to Si_3N_4 using NF_3/H_2/methanol chemistry was investigated. HF was formed using a NF_3/H_2 remote plasma, and in order to remove the F radicals, which induces spontaneous etching of Si-base material, methanol was injected outside the plasma discharge region. Through this process, etch products were formed on the surface of SiO_2, and then the $(NH_4)_2SiF_6$ was removed by following heating process. When the H and F radicals were abundant, the highest SiO_2 etch per cycle (EPC) was obtained. And, the increase of H_2 and methanol percentage in the gas chemistry increased the etch selectivity by decreasing the F radicals. The etch products such as $(NH_4)_2SiF_6$ were formed on the surfaces of SiO_2 and Si_3N_4 during the reaction step and no noticeable spontaneous etching by formation of SiF_4 was observed. By optimized conditions, the etch selectivity of SiO_2 over Si_3N_4 and poly Si higher than 50 and 20, respectively, was obtained while having SiO_2 EPC of ~ 13 nm/cycle. It is believed that the cyclic process using NF_3/H_2 remote plasma and methanol followed by heating can be applied to the selective isotropic SiO_2 etching of next generation 3D device fabrication.

SiO_2 films have been widely used in Si-based semiconductor devices together with Si_3N_4 films due to their excellent interfacial properties with Si, excellent dielectric properties, and easy processing[1]. These materials will be continuously used in next generation 3D semiconductor devices such as gate all around-field effect transistor (GAA-FET), and 3D memory devices, and, for these devices, highly selective isotropic etching processes in addition to highly selective anisotropic etching processes are required[2,3]. Currently, for selective isotropic etching of SiO_2 and Si_3N_4, wet etching processes using hydrofluoric acid (for etching of SiO_2) and phosphoric acid (for etching of Si_3N_4) are used[4,5]. However, wet etching processes may not be applicable for fabrication of next-generation devices of 10 nm or less due to the issues such as pattern leaning and collapsing caused by unbalanced capillary forces during drying of rinse liquid. In addition, since the etch rate is fast, it is difficult to control the process, and the problems might occur such as surface chemical damage by the etchant during etch process[6–8]. Therefore, it is necessary to develop selective isotropic dry etching processes that may solve these problems.

For a long time, gas-based SiO_2 etching processes have been applied to remove native SiO_2 layer formed on silicon wafer and thin SiO_2 layer at the bottom of contact hole and, to thin or remove SiO_2 hardmask layer. For isotropic dry etching of SiO_2 selective to Si_3N_4 and/or Si, a vapor process using HF vapor as HF source[9–14] and plasma processes forming HF by discharging F-based gases such as NF_3, SF_6, CF_4, OF_2, etc. and H-based gases such as NH_3, H_2, H_2O, etc. have been studied[15–21]. In these processes, since SiO_2 is hardly etched by anhydrous HF alone, a solvent that ionizes HF to react with SiO_2 is required, and the solvents such as H_2O, alcohol, NH_3, etc. have been used. By using H_2O or alcohol as a solvent, SiO_2 reacts with ionized HF (HF_2^-, HF, H^+, and F^-) in the solvent and forms volatile SiF_4[4,5,9,13]. For NH_3 as a solvent, SiO_2 is transformed into $(NH_4)_2SiF_6$ salt by the reaction of HF and NH_3, and the formed $(NH_4)_2SiF_6$ is decomposed into NH_3 and SiF_4 by heating at a temperature of 100 °C or higher[14–19]. Among these, the etching by HF ionization is known to be difficult to control the etch process because the etch rate is fast similar to the wet process, etch rate varies depending on the quality of the SiO_2 film, and additional rinse process may be necessary due to residual etchant[10,11,14]. So, HF/NH_3 vapor process and the NF_3/NH_3 plasma process are more widely used. However, ammonium salts such as NH_4F, NH_4HF_2 formed in the process using NH_3[15–19] can be a source of contamination in the chamber because they exist in the form

[1]School of Advanced Materials Science and Engineering, Sungkyunkwan University, Suwon 16419, Republic of Korea. [2]SKKU Advanced Institute of Nano Technology (SAINT), Sungkyunkwan University, Suwon 16419, Republic of Korea. [3]Department of Semiconductor Display Engineering, Sungkyunkwan University, Suwon 16419, Republic of Korea. [4]These authors contributed equally: Hong Seong Gil and Doo San Kim. ✉email: dwkim111@gmail.com; gyyeom@skku.edu

of solid powder at room temperature[22,23]. Therefore, to avoid direct reaction between NH_3 and HF in gaseous or plasma state, alternate SiO_2 dry etching processes have been investigated through reaction with NF_3 gas after inducing NH_3 formation through N_2/H_2 plasma[24] or through the formation of $(NH_4)_2SiF_6$ on SiO_2 by sequential supply of NH_3 gas after adsorption of HF from HF vapor or from plasmas generated with SF_6/H_2 or NF_3/H_2[25,26].

The above processes still use NH_3 gas or NH_3 formed through plasma which might generate particles, therefore, in this study, selective isotropic SiO_2 dry etching process not generating noticeable NH_3, by using H_2/NF_3 plasma as HF source and methanol (CH_3OH) vapor as a solvent, has been investigated. In order to minimize the generation of F radical during dissociation of NF_3 in the plasma which induces spontaneous etching of Si-base material[27], H_2/NF_3 gases were supplied to the remote plasma area and methanol were injected to the processing area located outside the plasma discharge region. And, dual grids separating the discharge area and the processing area were located to block the ions from the discharge area. Through a cyclic process, saturated etch products such as $(NH_4)_2SiF_6$ were formed on the surface of SiO_2, and then the etch products were removed by heating for precise control of etched SiO_2 thickness. The SiO_2 etch characteristics were measured according to process conditions such as gas ratio, pressure, temperature, and process time, and the etch selectivities over Si_3N_4 and poly Si were compared. The etch mechanism was investigated by analyzing plasmas, surface composition, etc.

Methods

200 nm thick SiO_2 deposited by low pressure chemical vapor deposition (LPCVD) on silicon wafers was used to measure the etch depth during the dry etching. 50 nm thick Si_3N_4 deposited on silicon wafers and 50 nm undoped poly silicon deposited on silicon oxide by LPCVD were used to measure the etch selectivity over SiO_2. In addition, trench patterned silicon wafers (80 nm top critical dimension (CD), 150 nm pitch, and 440 nm depth) sequentially deposited with 5 nm thick LPCVD-Si_3N_4 and 10 nm thick LPCVD-SiO_2 sequentially were used to investigate the etching effect on patterned samples. The quality of the Si_3N_4 used in this experiment was examined by wet etching in a HF solution (HF:deionized water = 1:100, RT) and the wet etch rates of Si_3N_4 and SiO_2 used in this experiment are shown in Supplementary Fig. S1. As shown in Fig. S1, the etch selectivity of SiO_2 over Si_3N_4 was ~ 50.

The isotropic dry etching system used in this study is shown in Fig. 1a,b. NF_3/H_2 gas mixture was supplied to the plasma area, and the plasma was generated by an inductively coupled plasma (ICP) source operated with 13.56 MHz radio frequency (RF) power. Two anodized aluminum grids with crossed holes were located below the plasma source to block ions and flow radicals only to the processing area, and methanol gas was supplied to the substrate through a shower ring located between the substrate and grids. The substrate temperature was controlled using a bath circulator (JEIO TECH, HTRC-10) and the substrate temperature was measured using a thermocouple in contact with the wafer. The base pressure of chamber was maintained at ~ 1×10^{-4} Torr using a dry pump (ALCATEL ADIXEN, ADS 602P).

The etching process was consisted of a reaction step using remote plasma and a removal step using heating as shown in Fig. 1c. During the reaction step, reacted etch products were formed on the surface of SiO_2 through radicals supplied from NF_3/H_2 plasmas through the grids and methanol vapor injected through the shower ring and, during the removal step, the formed etch products were removed by heating on a hot plate. For the reaction step, NF_3/H_2 plasma was formed with 500 W of RF power to the ICP source while maintaining the total operating pressure at 200 mTorr. Pressure ratios between NF_3 and H_2 gases in the plasma area and those between NF_3/H_2 gas mixture and methanol vapor were varied while keeping 200 mTorr. The substrate temperature was varied from 0 to 60 °C. For the removal step, formed etch products were removed by heating for 10 min. immediately after the plasma process on a hot plate (MTOPS, HSD180) preheated to 150 °C in a fume hood located next to the etcher. Also, the temperature and moisture of the etch room were controlled by using an air conditioning system.

Etch thicknesses of SiO_2, Si_3N_4, and poly Si were measured using an ellipsometer (Nano-View SE MG-1000). To understand the etching mechanism, an optical fiber was connected to a quartz window located on the top of the grid as shown in Fig. 1a, and gas species generated in the plasma were analyzed using optical emission spectroscopy (OES; Avantes, AvaSpec-3648). Radicals and recombined gas species outside the discharge region were analyzed through a residual gas analyzer (RGA; SRS, RGA200) located at the processing area below the grids. Gas phase Fourier transform-infrared spectroscope (FT-IR; MIDAC corporation, I2001) was connected to the exhaust end of the dry pump and the gases generated during the reaction steps were analyzed at the exhaust area while a 5×5 cm^2 sample located on the substrate holder was being processed. In addition, etch products formed on the blank samples and patterned samples were observed through field emission-scanning electron microscope (FE-SEM; HITACHI S-4700). Surface compositions and elemental bonding states of the SiO_2 and Si_3N_4 after each step were analyzed through X-ray photoelectron spectroscopy (XPS; Thermo VG, MultiLab 2000, Al Kα source) after peak shift based on C 1 s (~ 285 eV) and through Fourier transform-infrared spectroscopy (FT-IR; Thermo Electron Nicolet 5700), respectively. Also, the surface roughness for each step was analyzed using an atomic force microscope (AFM; Park System XE-100).

Results and discussion

For the cyclic etching, SiO_2, Si_3N_4, and poly Si were exposed to NF_3/H_2 remote plasma and methanol vapor for the formation of etch products (reaction step), and the etch products formed on the materials surface after the reaction were removed by heating at 150 °C for 10 min (removal step). The etch depth/cycle (EPC) of SiO_2, Si_3N_4, and poly Si and their etch selectivities were measured as functions of various reaction step parameters and the results are shown in Fig. 2. Figure 2a shows the EPCs and etch selectivities measured a function of NF_3/H_2 gas ratio. The partial pressure ratios between NF_3/H_2 and methanol were kept at 1:1 for total operating pressure of 200 mTorr. The RF power, substrate temperature, and process time were maintained at 500 W, 20 °C, and 20 min, respectively. As shown in Fig. 2a, the SiO_2 EPC was the highest at the ratio of NF_3:H_2 ~ 1:1 while the

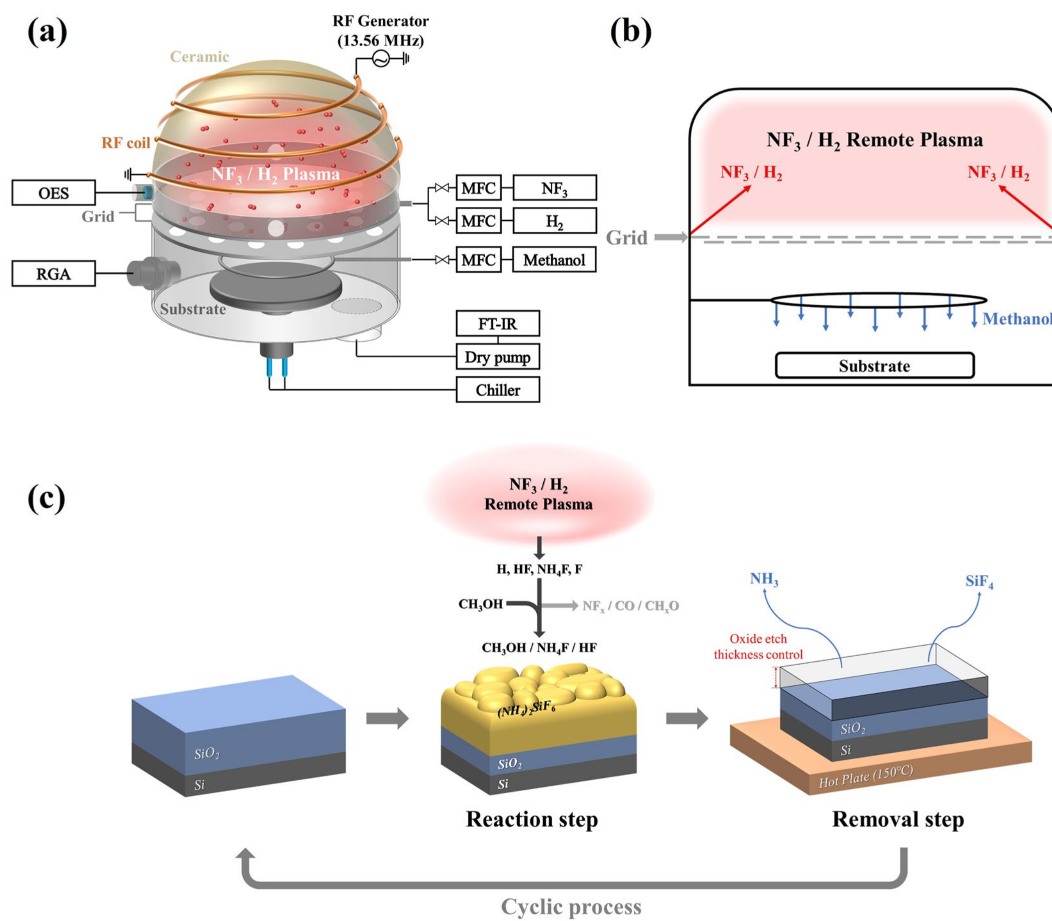

Figure 1. Schematic diagram of remote ICP type etcher and etch process steps. (**a**) Remote type ICP type etching system, (**b**) cross-sectional schematic diagram of the etcher with gas injections, and (**c**) cyclic etch process of SiO_2.

etch selectivity was increasing with increase of H_2 in the NF_3:H_2. While keeping the ratio between NF_3:H_2 ~ 1:3, the partial pressure ratio between NF_3/H_2 and methanol was also varied and the results are shown in Fig. 2b. Other process conditions were the same as those in Fig. 2a. (The EPCs as a function of the different partial pressure ratios between NF_3/H_2 and methanol for different ratios of NF_3:H_2 are also shown in Supplementary Fig. S2). The increase of partial pressure ratios of methanol from 1:0 (NF_3/H_2 only) to 1:5 decreased etch rates of all materials but increased the etch selectivity of SiO_2 over Si_3N_4 higher than 50 from the gas ratio of 1:5. With the ratio of NF_3:H_2 ~ 1:3 and the ratio of (NF_3/H_2): methanol ~ 1:3, the substrate temperature was varied from 0 to 60 °C while maintaining the other process conditions the same as Fig. 2a, and the etch results are shown in Fig. 2c. As shown in Fig. 2c, the decrease of substrate temperature increased EPC of SiO_2 possibly due to the increased adsorption on the materials surfaces while keeping the etch selectivity of SiO_2/Si_3N_4 higher than 50. When the plasma process time was varied for the optimized condition of the ratio of NF_3:H_2 ~ 1:3, the ratio of (NF_3/H_2):methanol ~ 1:3, and 0 °C, the SiO_2 EPC was saturated after ~ 10 min while keeping the etch selectivity over Si_3N_4 higher than 50. In the case of etch selectivity of SiO_2 over poly Si, the highest etch selectivity higher than 20 was also observed at the substrate temperature of 0 °C and the process time of 10 min for the ratio of NF_3:H_2 ~ 1:3 and the ratio of (NF_3/H_2): methanol ~ 1:3.

SiO_2 surface was exposed to the optimized reaction conditions of NF_3/H_2 (1:3):methanol ~ 1:3, the substrate temperature of 0 °C, and process time of 10 min (reaction step), and the etch products formed on the surface was observed by SEM before and after the reaction, and after the removal by heating at 150 °C for 10 min using a hot plate (removal step), and the results are shown in Fig. 3a–c. As shown in Fig. 3b, after the reaction step, etch products were observed on the SiO_2 surface and, after the removal step, the etch products formed on the SiO_2 surface were appeared to be removed. Tilted SEM images of the experimental results for Fig. 3b,c are shown in Fig. S3. While repeating the reaction and removal, the EPC and total etch depths were measured as a function of etch cycle and the result is shown in Fig. 3d. As shown in Fig. 3d, the EPC of SiO_2 was similarly remaining at ~ 13 nm/cycle, therefore, the total etch depth was linearly increased with cycle number not only for SiO_2 but also for all materials while keeping the SiO_2 etch selectivity over Si_3N_4 over 50.

To understand the EPC behavior observed in Fig. 2 as functions of various reaction parameters, the plasma characteristics in the plasma area and the species characteristics in reaction area under the grid were investigated

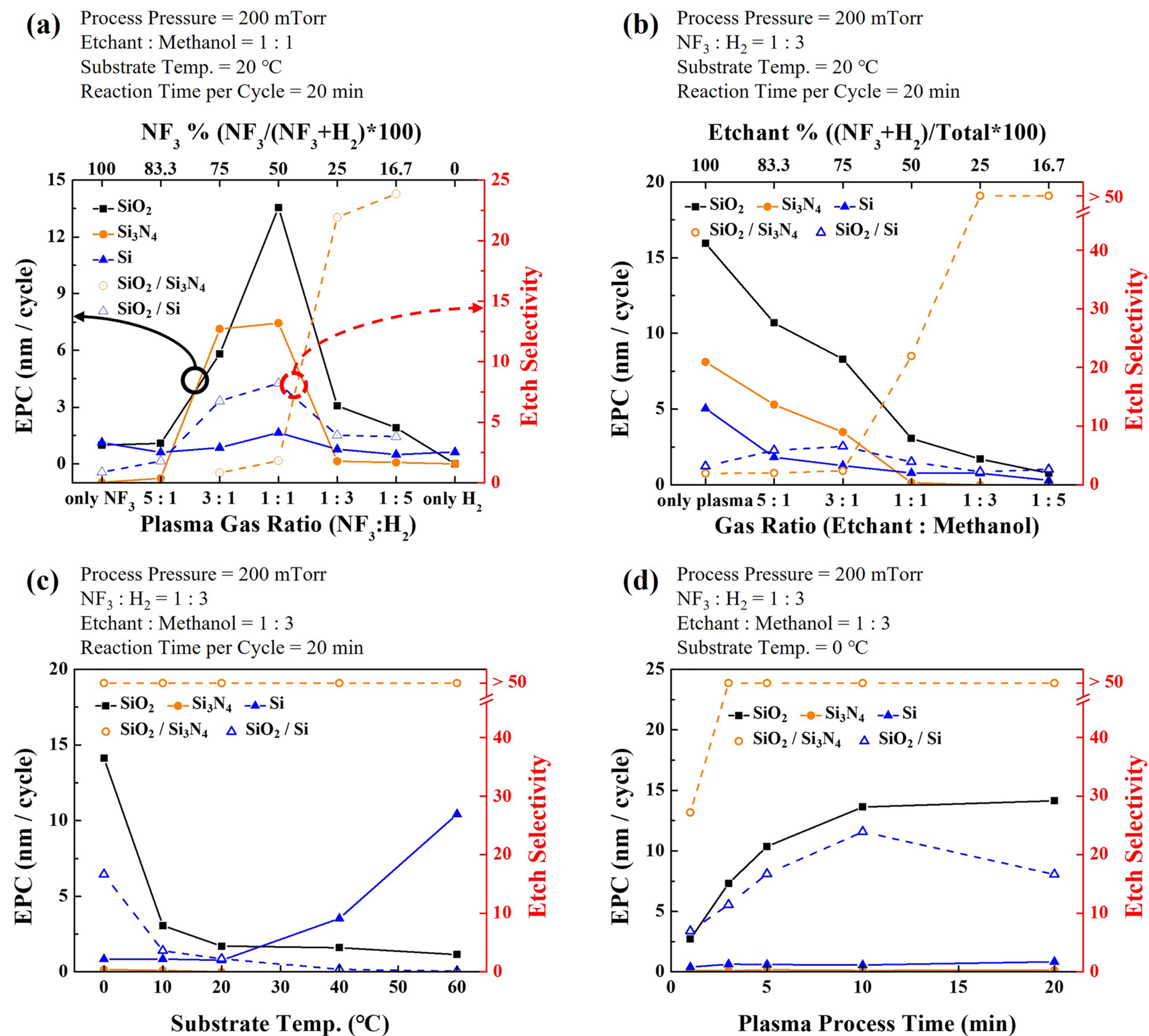

Figure 2. The EPC and etch selectivity of SiO_2, Si_3N_4, and poly Si as a function of (**a**) NF_3:H_2 gas pressure ratio, (**b**) NF_3/H_2:methanol pressure ratio, (**c**) substrate temperature, and (**d**) process time of reaction step.

using OES and RGA, respectively, and the results are shown in Fig. 4a,b for the condition in Figs. 2a and 4c,d for the condition in Fig. 2b. (OES spectra and RGA spectra can be found in Supplementary Figs. S4, S5 and S6, respectively) From OES, peaks related to H (656 nm), CO (519 nm), F (677 nm), NH or N (336 nm), and HF/CN/CH (388 nm) were observed, and, for the estimation of radical concentration, 10 mTorr of Ar was added during the OES measurement and the OES radical intensities were normalized by the Ar peak intensities at 750 nm. Figure 4a,c show the Ar normalized optical emission intensity ratios of species observed as a function of (a) NF_3:H_2 gas ratios and (c) NF_3/H_2:methanol ratios. As shown in Fig. 4a, with increasing H_2 ratio, the increase of H intensity was observed while, with increasing NF_3, the increase of F and N-related (NH or N_2) peaks were observed due to the increase of related molecules in the gas mixture. Also, as shown in Fig. 4c, the increase of NF_3/H_2 in NF_3/H_2:methanol increased F, H, and N-related peaks while the increase of methanol in NF_3/H_2:methanol increased the CO also due to the increase of related molecules in the gas mixture. In addition, even though no hydrogen exists for NF_3:H_2 = 1:0 in Fig. 4a, H in addition to CO was detected in the plasma area and, as shown in Fig. 4c, even with decrease of H_2 with increasing methanol, H did not decrease linearly possibly due to the formation of H through decomposition of methanol penetrated into the plasma area. Especially, as shown in Fig. 4a, c, the highest HF (or CN, CH but from Fig. 4b, it appears to be more related to HF) peak intensity was observed with the adequate mixture of NF_3 and H_2 possibly due to the highest formation HF from sufficient H and F in the plasma.

For RGA measured at the reaction area, masses such as H_2 (2 amu), H_2O (18 amu), HF (29 amu), CO or N_2 (28 amu), CH_2OH/CH_3OH (31/32 amu), CF_3 (69 amu), NF_3 (71 amu), etc. were observed. However, highly reactive H (1 amu) and F (19 amu) radicals observed by OES in the plasma area were hardly measured in the

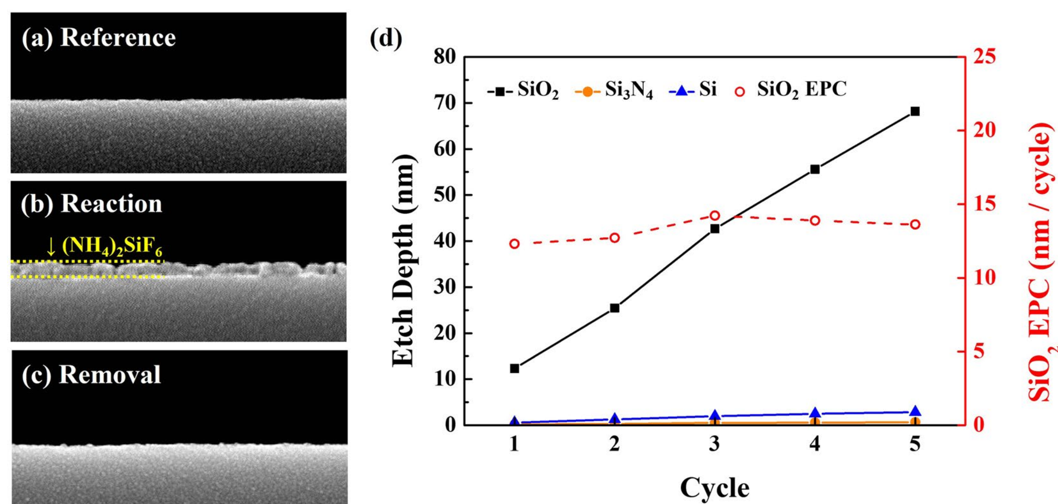

Figure 3. SEM images of SiO_2 surface; (**a**) for reference, (**b**) after reaction step, and (**c**) after removal step. (**d**) Etch depth and EPC for 5 etch cycles. SiO_2 surface was exposed to the optimized reaction conditions of NF_3/H_2 (1:3):methanol ~ 1:3, the substrate temperature of 0 °C, and process time of 10 min (reaction step), and the etch product formed on the surface was observed by SEM before and after the reaction, and after the removal by heating at 150 °C for 10 min using a hot plate (removal step).

reaction area by RGA due to recombination during the gas transportation from the plasma area to the reaction area. Figure 4b,d show the mass peak intensities observed as a function of (b) NF_3:H_2 gas ratios and (d) NF_3/H_2:methanol ratios for the conditions in Fig. 4a,c, respectively. As shown in Fig. 4b,d, with the increase of H_2 in NF_3:H_2 and with the increase of NF_3/H_2 in NF_3/H_2:methanol, the increase of H_2 was observed in the reaction area by RGA, while the increase of NF_3 in NF_3:H_2 and the increase of methanol in NF_3/H_2:methanol increased CO/N_2 possibly due to the reaction of CH_3OH with F from NF_3 and dissociation of CH_3OH. HF molecules were observed by RGA in the reaction area as shown in Fig. 4b,d, and the HF molecules showed the highest peak with the adequate mixture of NF_3:H_2 at the reaction area and at the ratio of NF_3/H_2:methanol = 1:0 similar to the SiO_2 etch results shown in Fig. 2a,b, respectively. Therefore, it is believed that, HF molecules formed by reaction of F with H (from H_2 and decomposed CH_3OH) in the plasma area and diffused to the reaction area are related to the SiO_2 EPC observed in Fig. 2a,b.

While etching SiO_2 with the conditions in Fig. 2a,b, the recombined species and etch products were observed using gas phase FT-IR located at the exhaust area. The species observed by gas phase FT-IR are shown in Fig. 5a for NF_3:H_2 gas ratios and (b) for NF_3/H_2: methanol ratios. Species such as CH_3OH, CO, CH_4, NF_3, NH_3, and HF were observed at the exhaust area by FT-IR. However, species such as H_2, N_2, O_2 etc. could not be observed or measured by using FT-IR because these species do not absorb IR due to no changing dipole moments during the vibration that allow for the absorption of photons. As shown in Fig. 5, the variation of species observed by gas phase FT-IR with NF_3:H_2 gas ratios and NF_3/H_2:methanol ratios was similar to RGA data possibly due to the transport of recombined species without significant reaction from reaction area to the exhaust area. The FT-IR results obtained during the etching of Si_3N_4 and poly Si (not shown) under the same conditions as those obtained during the SiO_2 etching were the same as Fig. 5a,b, and no SiF_4 or SiH_4 was also observed under all conditions. Therefore, it indicates that, during the reaction step, no noticeable spontaneous etching of SiO_2, Si_3N_4, and poly Si with the reaction gases such as F and H in the reaction area was occurred.

The reaction compounds on the surfaces of SiO_2 and Si_3N_4 after reaction step and removal step for the different NF_3:H_2 ratios were observed by SEM and the results are shown in Figs. 6 and 7 for SiO_2 and Si_3N_4, respectively. The process conditions are the same as those in Fig. 2a. As shown in Fig. 6, after the reaction step, the reaction products formed on the surface were observed and, for high etch rate condition of NF_3:H_2 ~ 1:1, the thickest reaction product was observed. And, after the removal step, no noticeable reaction products on the SiO_2 surface could be observed for all etch conditions. In case of Si_3N_4, as shown in Fig. 7, the thickest reaction product was also observed at the highest Si_3N_4 etch condition of NF_3:H_2 ~ 1:1, and after the removal step, no reaction products were observed on the Si_3N_4 surface for all etch conditions. Because no etch products such as SiF_4 were observed during the reaction step as observed by gas phase FT-IR while forming the thickest reaction product at the condition of highest etch rate conditions, the reaction products were formed on the surfaces of Si_3N_4 and SiO_2 during the reaction step without spontaneous etching of Si_3N_4 and SiO_2 by F radicals and the reaction products were removed by heating during the removal step during the removal step. In fact, even with high F concentration for the condition of NF_3:H_2 = 1:0 as shown in Fig. 4a, no spontaneous etching of Si_3N_4 and SiO_2 was observed as shown in Fig. 2a. From the data from OES, RGA, and gas phase FT-IR in Figs. 4 and 5, it is believed that F radicals formed from dissociation in the plasma area react with methanol (CH_3OH) in the reaction area to form HF according to the formula below[28,29];

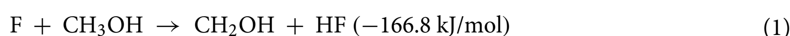

$$F + CH_3OH \rightarrow CH_2OH + HF \ (-166.8\ \text{kJ/mol}) \tag{1}$$

Figure 4. OES and RGA data as a function of (**a**,**b**) NF_3:H_2 pressure ratio and (**c**,**d**) NF_3/H_2:methanol pressure ratio. (**a**,**b**) are for the condition in Fig. 2a,c,d are for the condition in Fig. 2b.

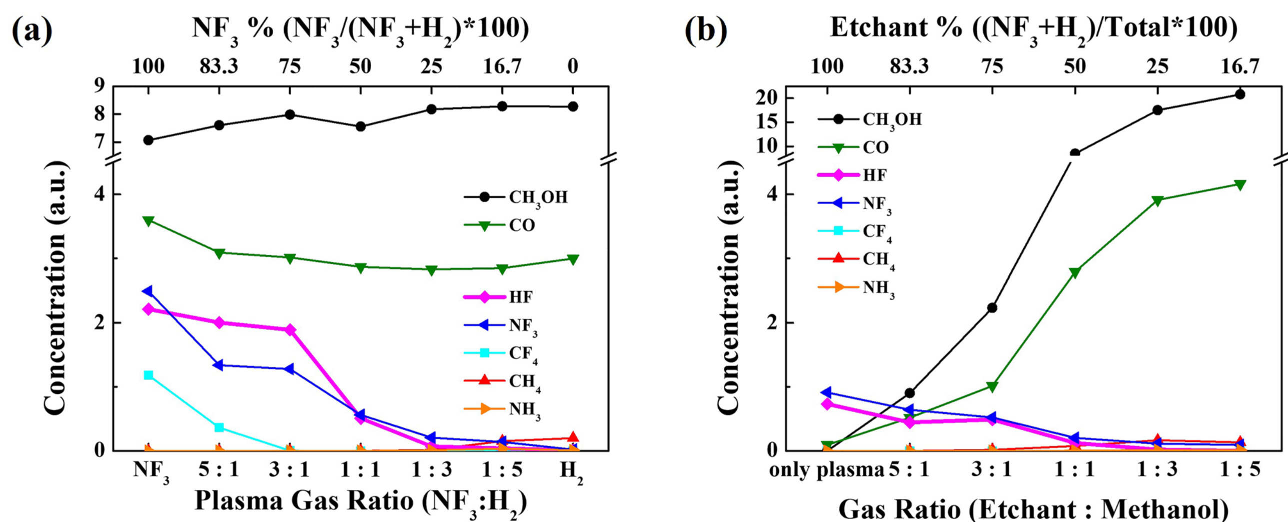

Figure 5. Gas phase FT-IR data measured as a function of (**a**) NF_3:H_2 pressure ratio and (**b**) NF_3/H_2:methanol pressure ratio for the process conditions in Fig. 2a,b, respectively.

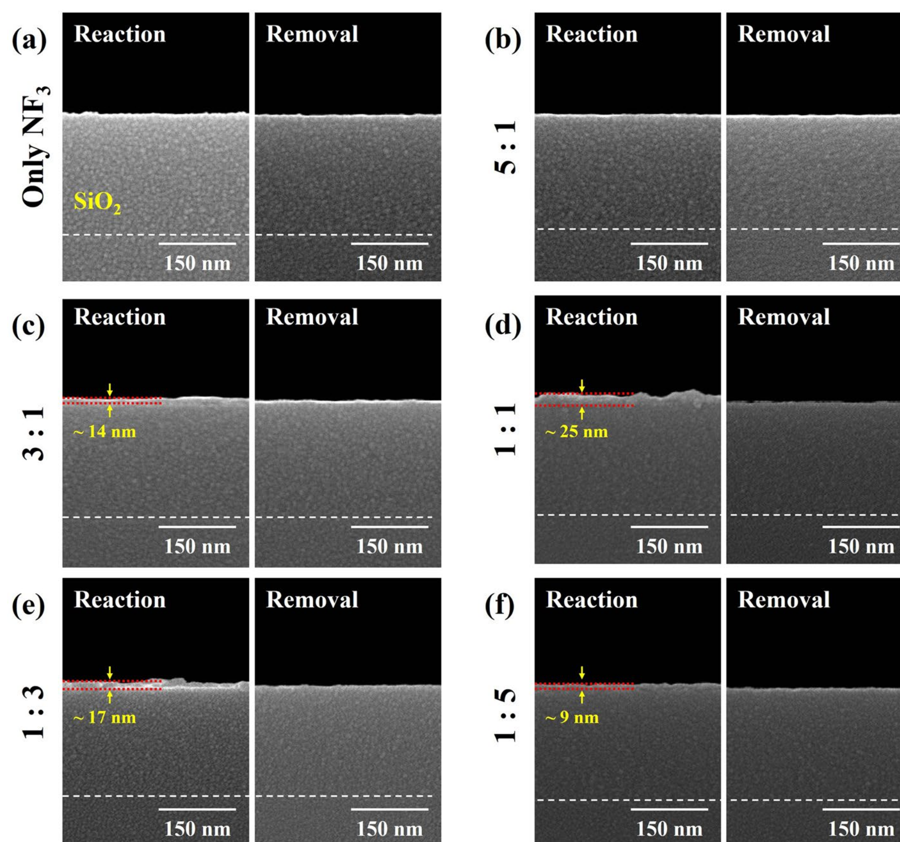

Figure 6. SEM images of SiO_2 surface after reaction and removal steps according to NF_3:H_2 pressure ratio from NF_3 only (1:0) to 1:5. The process conditions are same as those in Fig. 2a.

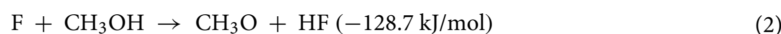

$$F + CH_3OH \rightarrow CH_3O + HF\ (-128.7\ \text{kJ/mol}) \quad (2)$$

Therefore, no spontaneous etching of SiO_2 and Si_3N_4 is appeared to be observed even with high concentration of F radicals in the plasma area. Some methanol also can participate in the discharge and is decomposed into H and CO, so it could act as H donor for HF formation for F radicals in the plasma area[30,31]. The increase of etch selectivity of SiO_2 over Si_3N_4 obtained with the increase ratios of methanol in NF_3/H_2:methanol is also believed to be related to the formation of HF through the reaction of F with methanol.

To find out the materials characteristics of the reaction products formed on the surfaces of SiO_2 and Si_3N_4, the surface characteristics were measured by XPS, FT-IR, and AFM. The process conditions are the same as those in Fig. 3. Figure 8 shows (a, d) atomic composition and narrow scan data of (b, e) N 1 s and (c, f) F 1 s for the surfaces of (a–c) SiO_2 and (d–f) Si_3N_4 measured by XPS before (reference) and after reaction step, and after removal step with the optimized etch condition (XPS wide scan data of the surfaces of SiO_2 and Si_3N_4 during the process steps are shown in Supplementary Fig. S7). As shown in Fig. 8a, for SiO_2, after the reaction, the atomic percentages of Si and O were decreased from 36.1 to 12.7% and from 59.1 to 2.6%, respectively, while showing 54.7% of F after the reaction. The atomic percentage ratio between N and F in the etch product after the reaction was similar to $(NH_4)_2SiF_6$. In the case of Si_3N_4, as shown in Fig. 8d, after the reaction, the atomic percentages of Si and N were slightly decreased from 42.6 to 35% and from 12.8 to 6.9% respectively, while showing 12.8% of F after the reaction due to the etch product formation similar to SiO_2 even though the etch product thickness on Si_3N_4 was much thinner than that on SiO_2. However, after the removal step, the surface compositions of both SiO_2 and Si_3N_4 were almost recovered similar to those of references due to the removal of reaction products formed on the surfaces. Also, as shown in Fig. 8b,c,e,f, after the reaction step, the formation of etch products composed of N–H–Si–F could be identified for both SiO_2 and Si_3N_4 by forming N–H bonding at 402 eV and Si–F bonding at 685 eV after the reaction step and, after the removal step, the removal of the etch products by removing those peaks. In addition, on the samples surfaces, ~ 10.9, 7.8% of carbon for SiO_2 and Si_3N_4 and ~ 7.4% of oxygen for Si_3N_4 were continuously observed possibly due to the contamination and oxidation, respectively, due to the air exposure during the transport to XPS.

The binding states of etch products formed on the surfaces of SiO_2 and Si_3N_4 after the reaction/removal steps using the optimized conditions of Fig. 3 were also observed using FT-IR and the results are shown in Fig. 9a,b, respectively. As shown in Fig. 9a, for SiO_2, the absorption peaks such as N–H stretching (3330 cm^{-1}), N–H bending (1454 cm^{-1}) related to NH_4^+ bonding, and SiF_6^{2-} bonding (717 cm^{-1}, 478 cm^{-1}) were observed after the

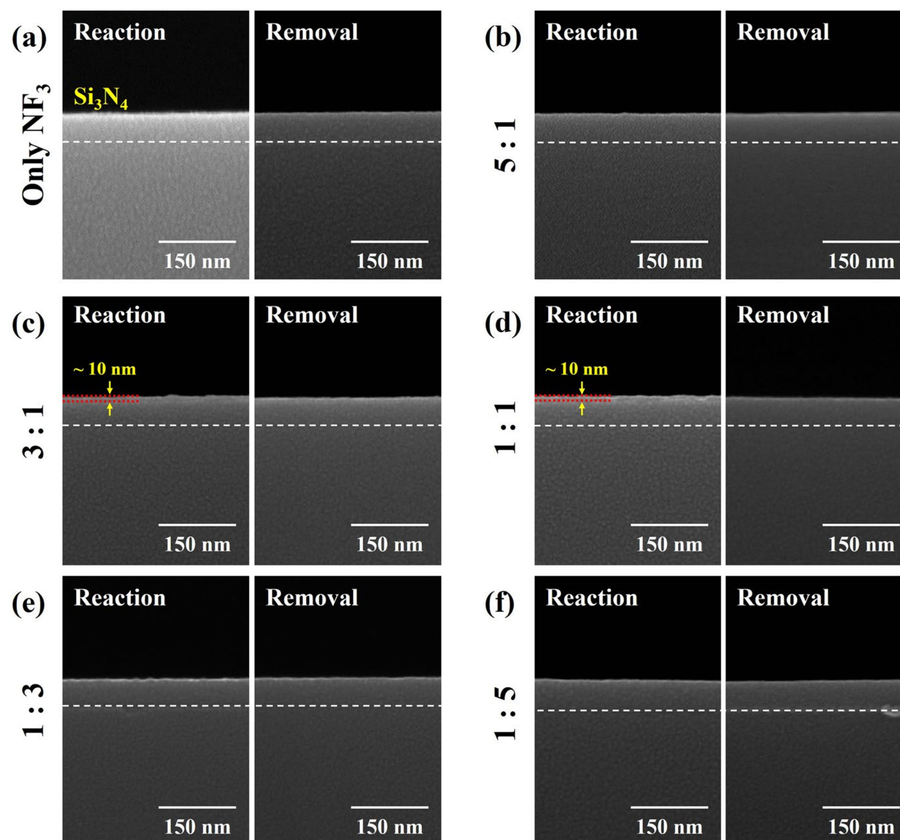

Figure 7. SEM images of Si_3N_4 surface after reaction and removal steps according to NF_3:H_2 pressure ratio from NF_3 only (1:0) to 1:5. The process conditions are same as those in Fig. 2a.

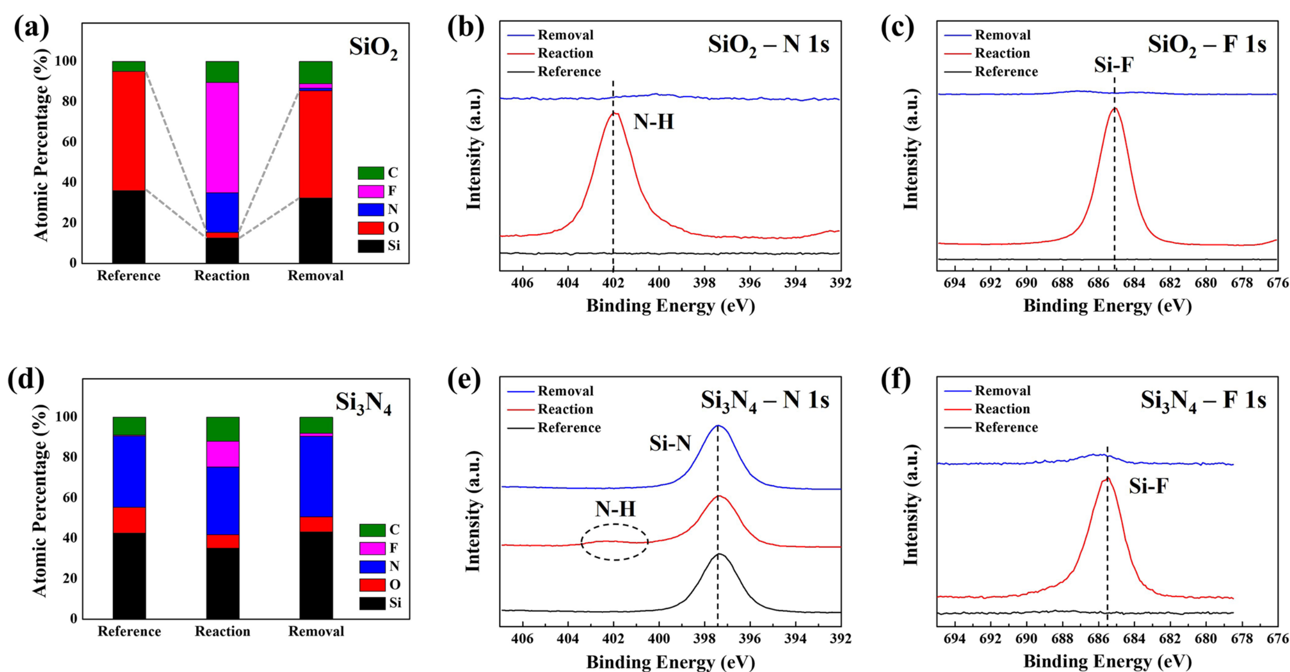

Figure 8. XPS analysis data for each process step under optimized conditions in Fig. 3; (**a**) atomic percentages of SiO_2 surface for each process step, (**b**) N 1 s narrow scan of SiO_2 surface, (**c**) F 1 s narrow scan of SiO_2 surface, (**d**) atomic percentages of Si_3N_4 surface for each process step, (**e**) N 1 s narrow scan of Si_3N_4 surface, and (**f**) F 1 s narrow scan of Si_3N_4 surface.

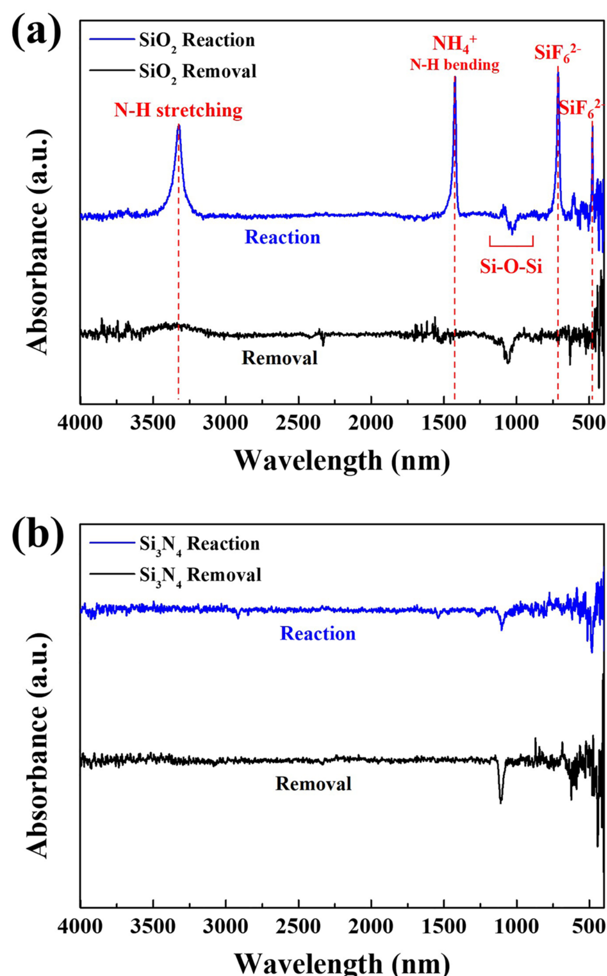

Figure 9. FT-IR analysis data for each process step under optimized conditions in Fig. 3; (**a**) FT-IR analysis result of SiO_2 after reaction and removal steps and (**b**) FT-IR analysis result of Si_3N_4 after reaction and removal steps.

reaction and, by comparing the XPS results in Fig. 8, it could be concluded that the etch products formed on the SiO_2 surface after the reaction were related to $(NH_4)_2SiF_6$. However, in case of Si_3N_4, as shown in Fig. 9b, possibly due to very thin etch product formation, no noticeable absorption peaks such as Si–F bonding related to etch products could be observed. In addition, after the removal steps, as shown in Fig. 9a,b, no absorption peaks could be also observed due to the removal of the etch product formed on the surfaces of both SiO_2 and Si_3N_4. The XPS and FT-IR were also measured for poly Si and the results are shown in Supplementary Fig. S8. From the above observations, it is believed that the alkaline salt etch products such as $(NH_4)_2SiF_6$ are formed by following reactions;

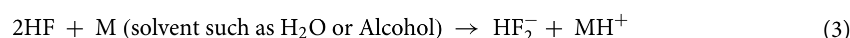

$$2HF + M\ (\text{solvent such as } H_2O \text{ or Alcohol}) \rightarrow HF_2^- + MH^+ \quad (3)$$

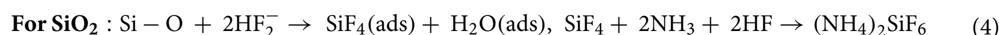

$$\textbf{For SiO}_2: Si - O + 2HF_2^- \rightarrow SiF_4(ads) + H_2O(ads),\ SiF_4 + 2NH_3 + 2HF \rightarrow (NH_4)_2SiF_6 \quad (4)$$

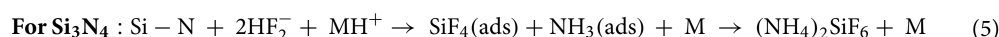

$$\textbf{For Si}_3\textbf{N}_4: Si - N + 2HF_2^- + MH^+ \rightarrow SiF_4(ads) + NH_3(ads) + M \rightarrow (NH_4)_2SiF_6 + M \quad (5)$$

In the above reactions, the formation of H_2O for SiO_2 etching and the formation of NH_3 for Si_3N_4 etching can be important and the differences in etch rates, that is, differences in the etch product thickness could be related to the differences in the free energy of formation of H_2O (− 265 kJ/mol) and NH_3 (− 33.2 kJ/mol).

For the optimized conditions in Fig. 3, the change of surface roughness values during the each step of cyclic processing was observed using AFM and the RMS surface roughness values observed for SiO_2, Si_3N_4, and poly Si are shown in Fig. 10a up to 5 cycles of etching and the 2D AFM surface roughness images of references, after reaction step, and after removal step for SiO_2 and Si_3N_4 during 1st cycle of etching are shown in Fig. 10b–g. As shown in Fig. 10a,b–d, in the case of SiO_2, after the reaction, the RMS surface roughness was significantly

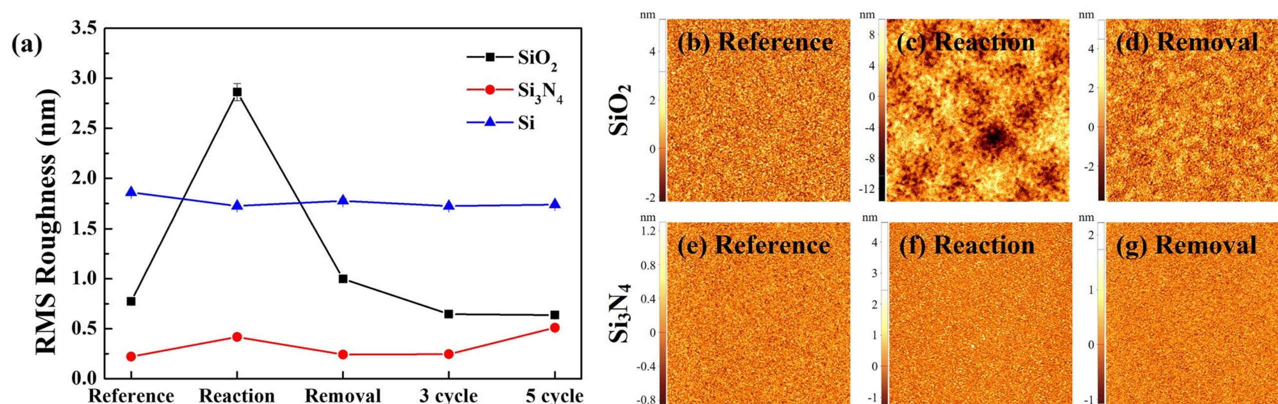

Figure 10. AFM analysis for each process step under optimized conditions in Fig. 3; (**a**) RMS roughness change of SiO_2, Si_3N_4, and poly Si for 5 etch cycles. (**b**–**g**) AFM scan images of reference, after reaction step, and after removal step of SiO_2 and Si_3N_4.

increased from 0.77 to 2.86 nm due to the formation of etch product such as $(NH_4)_2SiF_6$. However, after the removal step, the RMS surface roughness was decreased to ~ 1.0 nm, and, even after 5 cycles of etching, the RMS surface roughness remained similar to that of reference. In the case of Si_3N_4, as shown in Fig. 10a,e–g, due to the very thin etch product formation during the reaction step, only slight increase of surface roughness from 0.22 to 0.42 was observed during the reaction step and, after the removal step, the RMS surface roughness was also decreased similar to that of the reference and no significant change was observed up to 5 cycles of etching. In the case of poly Si, possibly due to no formation of etch product similar to $(NH_4)_2SiF_6$ during the reaction step, no significant change in RMS surface roughness was observed during the each step of etching. Therefore, on the surfaces of SiO_2, Si_3N_4, and poly Si, no noticeable physical damage was observed by the cyclic etching.

The optimized SiO_2 cyclic etching selective to Si_3N_4 was applied to a patterned sample and the results are shown in Fig. 11. Figure 11a shows the schematic drawing of a patterned Si sample having the aspect ratio of ~ 10 and sequentially deposited with 5 nm thick Si_3N_4 and 10 nm thick SiO_2. Actual SEM images of Si pattern after deposition of 5 nm thick Si_3N_4 and after following deposition of 10 nm thick SiO_2 are shown in Fig. 11c,d, respectively. After the deposition of 5 nm thick Si_3N_4, the top/bottom CDs were ~ 60 nm/105 nm, and after the following deposition of 10 nm thick SiO_2 (reference), the top/bottom CDs were changed to ~ 80 nm/115 nm. The Si trench pattern sample deposited with Si_3N_4/SiO_2 was etched using the optimized condition in Fig. 3 and Fig. 11e,f show the SEM images after the reaction step and after the following removal step, respectively. As shown in Fig. 11e, after the reaction, due to the formation of reaction product, the top/bottom CDs were increased to ~ 100/125 nm, and the reaction product thickness was thicker on the top area (the byproduct thickness at the top of the trench was ~ 27.85 nm and that at the bottom of the trench was ~ 12.67 nm as shown in Fig. 11e). As shown in Fig. 11f, after the removal step, the etch product appeared to be removed and, the top/bottom CDs were decreased to ~ 60/111 nm. Due to the thinner etch product formation at the trench bottom area, three cycles were required to remove all SiO_2 deposited on the Si pattern sample as shown in Fig. 11g,h. The measured top/bottom CDs are shown in Fig. 11b and, after the 3 cycles, the top/bottom CDs were the same as those of Si pattern deposited with 5 nm thick Si_3N_4, therefore, isotropic SiO_2 etching selective to Si_3N_4 could be verified in a high aspect ratio patterned sample.

Conclusions

In this study, isotropic dry etching of SiO_2 selective to Si_3N_4 and poly Si was carried out using a two-step cyclic process composed of the etch products formation on SiO_2 surface by using NF_3/H_2 remote plasma and methanol vapor, and the thermal desorption of the etch products by heat treatment. By using the cyclic process, ~ 13 nm/cycle of SiO_2 etch per cycle (EPC) with the etch selectivity over Si_3N_4 higher than 50 for Si_3N_4 and that over poly Si higher than 20 could be obtained. The highest EPCs of SiO_2 and Si_3N_4 were obtained when both H and F are abundant and the higher etch selectivity of SiO_2 over Si_3N_4 could be obtained when H is richer than F in the system. Especially, methanol acted as H donor for HF formation for F radicals in the plasma area, therefore, the increase of methanol in the gas mixture increased the etch selectivity of SiO_2 over Si_3N_4 even though the EPC of SiO_2 decreased with increasing the methanol percentage. The etching of both SiO_2 and Si_3N_4 was processed by formation and removal of etch products such as $(NH_4)_2SiF_6$ not by forming volatile SiF_4. When a silicon nanoscale trench patten sequentially deposited with Si_3N_4 and SiO_2 was etched by the isotropic etching method, only SiO_2 was etched on the nanoscale trench pattern by exposing silicon pattern surface deposited with Si_3N_4. Therefore, it is believed that this process can be applied for the selective isotropic etching of SiO_2 for the next generation 3D devices, etc. Especially, by the formation of HF in the plasma without using the NH_3 for the isotropic etching of SiO_2, the formation of particles caused by NH_3 is expected to be minimized.

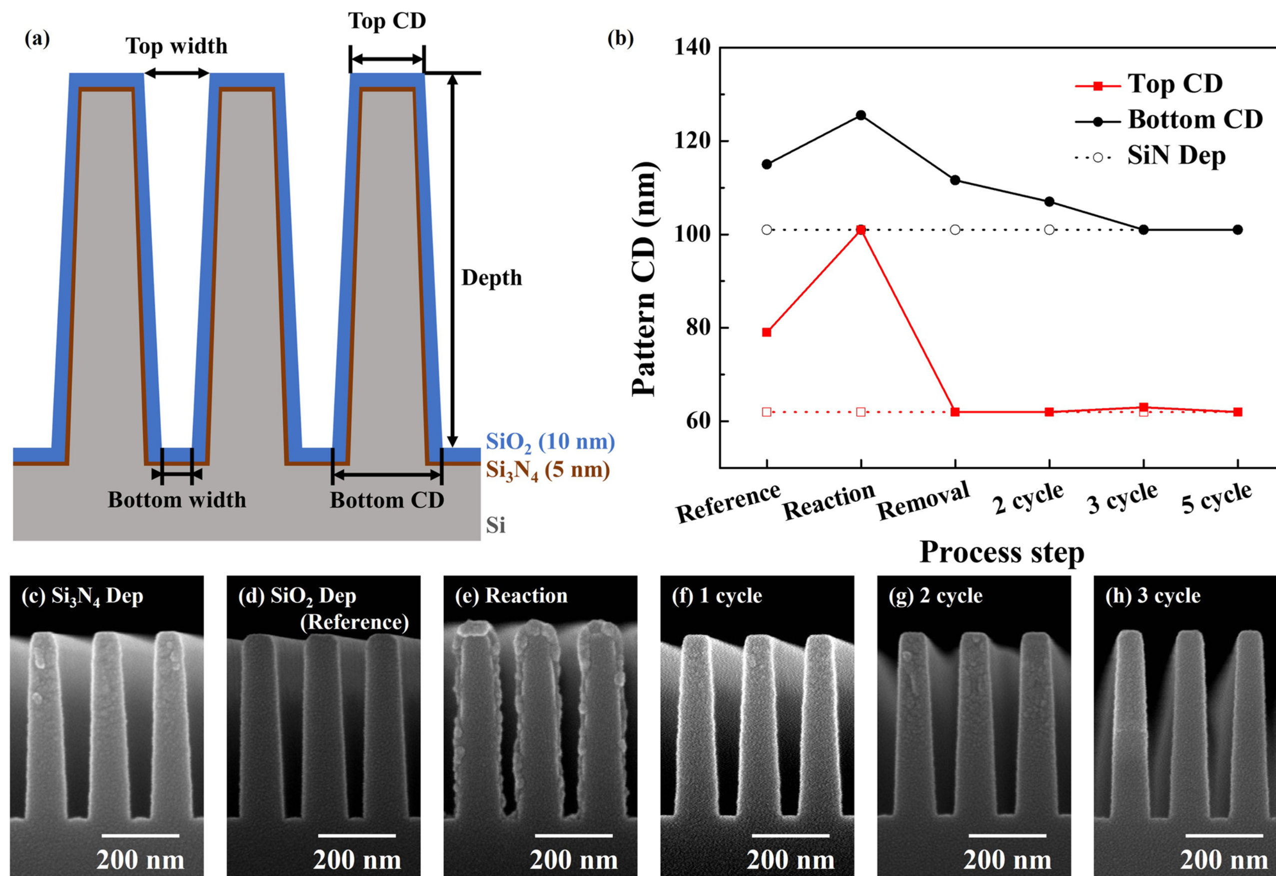

Figure 11. Etching of patterned silicon sample sequentially deposited with 5 nm thick Si_3N_4 and 10 nm thick SiO_2 using the optimized etching conditions in Fig. 3; (**a**) schematic diagram of patterned sample reference, (**b**) CD change during process steps and cycles, and (**c**–**h**) SEM image of (**c**) after 5 nm Si_3N_4 deposition on Si trench, (**d**) after 5 nm Si_3N_4/10 nm SiO_2 deposition (reference), (**e**) after reaction of 1st cycle, (**f**) after removal of 1st cycle, (**g**) after 2nd cycle, and (**h**) after 3rd cycle.

Data availability

Data will be made available on request to Geun Young Yeom. (gyyeom@skku.edu).

Received: 17 May 2023; Accepted: 6 July 2023
Published online: 18 July 2023

References

1. Kaloyeros, A.E., Pan, Y., Goff, J., & Arkles, B. Review—silicon nitride and silicon nitride-rich thin film technologies: state-of-the-art processing technologies, properties, and applications. *ECS J. Solid State Sci. Technol.* **9**, 063006. https://doi.org/10.1149/2162-8777/aba447 (2020).
2. Mukesh, S., & Zhang, J. A review of the gate-all-around nanosheet FET process opportunities. *Electronics* **11**, 3589. https://doi.org/10.3390/electronics11213589 (2022).
3. Fischer, A., Routzahn, A., George, S. M., & Lill, T. Thermal atomic layer etching: A review. *J. Vac. Sci. Technol. A*. **39**, 030801. https://doi.org/10.1116/6.0000894 (2021).
4. Spierings, G. A. C. M. Wet chemical etching of silicate glasses in hydrofluoric acid based solutions. *J. Mater. Sci.* **28**, 6261–6273 (1993).
5. Williams, K. R. & Muller, R. S. Etch rates for micromachining processing. *J. Microelectromech. Syst.* **5**, 256–269 (1996).
6. Kohli, R., & Mittal, K. L. *Developments in Surface Contamination and Cleaning: Methods for Surface Cleaning Volume 9*, 1st Edition, (Elsevier, 2017).
7. Toshima, T., Nishikido, S., Yamasaka, M. & Suni, K. Single wafer wet clean challenges and solution for 32nm. *ECS Trans.* **44**, 305–311 (2012).
8. Shariar, K. F. *et al.* The effects of ICP dry etching and HF wet etching on the morphology of SiO_2 surface. *Mater. Res. Express.* **5**, 095903. https://doi.org/10.1088/2053-1591/aad591 (2018).
9. Helms, C. R. & Deal, B. E. Mechanisms of the HF/H_2O vapor phase etching of SiO_2. *J. Vac. Sci. Technol. A*. **10**, 806–811 (1992).
10. Torek, K., Ruzyllo, J., Grant, R. & Novak, R. Reduced pressure etching of thermal oxides in anhydrous HF/alcoholic gas mixtures. *J. Electrochem. Soc.* **142**, 1322–1326 (1995).
11. Witvrouw, A. *et al.* Comparison between wet HF etching and vapor HF etching for sacrificial oxide removal. *Proc. SPIE.* **4174**, 130–141 (2000).
12. Shimaoka, K., Funabashi, H. & Mitsushima, Y. Characteristics of silicon nitride reaction to vapor-phase HF gas treatment. *IEEJ Trans. Sens. Micromach.* **126**, 516–521 (2006).

13. Guillemin, S. *et al.* Etching mechanisms of SiO_2 and SiN_x: H thin films in HF/Ethanol vapor phase: Toward high selectivity batch release processes. *J. Microelectromech. Syst.* **28**, 717–723 (2019).
14. Hagimoto, Y. *et al.* Evaluation of the plasmaless gaseous etching process. *Solid State Phenom.* **134**, 7–10 (2008).
15. Nishino, H., Hayasaka, N. & Okano, H. Damage-free selective etching of Si native oxides using NH_3/NF_3 and SF_6/H_2O down-flow etching. *J. Appl. Phys.* **74**, 1345–1348 (1993).
16. Ogawa, H., Arai, T., Yanagisawa, M., Ichiki, T. & Horiike, Y. Dry cleaning technology for removal of silicon native oxide employing Hot NH_3/NF_3 exposure. *Jpn. J. Appl. Phys.* **41**, 5349–5358 (2002).
17. Kim, H. T. *et al.* Investigation of oxide layer removal mechanism using reactive gases. *Microelectron. Eng.* **135**, 17–22 (2015).
18. Park, J. W. *et al.* In situ dry cleaning of Si wafer using OF_2/NH_3 remote plasma with low global warming potential. *J. Phys. D: Appl. Phys.* **51**, 445201. https://doi.org/10.1088/1361-6463/aae182 (2018).
19. Cho, Y. G., Kim, Y. J., Kim, S. J., & Chae, H. Y. Atomic layer etching of SiO_2 for surface cleaning using ammonium fluorosilicate with CF_4/NH_3 plasma. *J. Vac. Sci. Technol. A.* **38**, 022604. https://doi.org/10.1116/1.5132986 (2020).
20. Kikuchi, J., Iga, M., Ogawa, H., Fujimura, S. & Yano, H. Native oxide removal on Si surfaces by NF_3-added hydrogen and water vapor plasma downstream treatment. *Jpn. J. Appl. Phys.* **33**, 2207–2211 (1994).
21. Yamakawa, K. *et al.* Etching process of silicon dioxide with nonequilibrium atmospheric pressure plasma. *J. Appl. Phys.* **98**, 013301. https://doi.org/10.1063/1.1944219 (2005).
22. Ammonium fluoride, *PubChem,* https://pubchem.ncbi.nlm.nih.gov/compound/25516 (2005).
23. Ammonium bifluoride, *PubChem,* https://pubchem.ncbi.nlm.nih.gov/compound/14935 (2005).
24. Miyatani, K., Nishizawa, K., Kobayashi, Y., Tada, Y. A new plasma dry cleaning method applied to contact and gate pre cleaning. *ICSSDM.* 196–197 (2002).
25. Gill, Y. J. *et al.* Cyclic etching of silicon oxide using NF_3/H_2 remote plasma and NH_3 gas flow. *Plasma Process. Polym.* **18**, 2100063. https://doi.org/10.1002/ppap.202100063 (2021).
26. Miyoshi, N. *et al.* Atomic layer etching of SiO_2 with self-limiting behavior on the surface modification step using sequential exposure of HF and NH_3. *J. Vac. Sci. Technol. A.* 40 012601. https://doi.org/10.1116/6.0001517 (2022).
27. Donnelly, V. M. Review article: Reactions of fluorine atoms with silicon, revisited, again. *J. Vac. Sci. Technol. A.* **35**, 05C202. https://doi.org/10.1116/1.4983922 (2017).
28. Assaf, E., Schoemaecker, C., Vereecken, L. & Fittschen, C. The reaction of fluorine atoms with methanol: Yield of CH_3O/CH_2OH and rate constant of the reactions CH_3O+CH_3O and CH_3O+HO_2. *Phys. Chem. Chem. Phys.* **20**, 10660–10670 (2018).
29. Lu, D., & Li, J. Mode specificity of a multi-channel reaction prototype: $F+CH_3OH \rightarrow HF+CH_3O/CH_2OH$, *Theor. Chem. Acc.* **139**, 157. https://doi.org/10.1007/s00214-020-02671-3 (2020).
30. Zhang, H. *et al.* Non-oxidative decomposition of methanol into hydrogen in a rotating gliding arc plasma reactor. *Int. J. Hydrog. Energy.* **40**, 15901–15912 (2015).
31. Zhang, H., Zhu, F., Bo, Z., Cen, K. & Li, X. Hydrogen production from methanol decomposition in a gliding arc discharge plasma with high processing capacity. *Chem. Lett.* **44**, 1315–1317 (2015).

Acknowledgements

This study was supported by the Technology Innovation Program (or Industrial Strategic Technology Development Program—The Development of next-generation intelligent semiconductor technology) (20012609, Atomic Layer Etching Solution and System for Real Time Process Control) funded By the Ministry of Trade, Industry & Energy (MOTIE, Korea) and Samsung Electronics Co., Ltd. (IO201211-08086-01).

Author contributions

G.Y.Y. and D.W.K. initiated the project. H.S.G., D.S.K. and G.Y.Y. contributed to the experimental design. H.S.G. and D.S.K. wrote the main manuscript text. Y.J.J. and D.W.K. contributed to the data analysis. Y.J.J., H.I.K. and G.C.K. contributed to the experimental setup. All authors reviewed the manuscript.

Competing interests

The authors declare no competing interests.

Additional information

Supplementary Information The online version contains supplementary material available at https://doi.org/10.1038/s41598-023-38359-4.

Correspondence and requests for materials should be addressed to D.W.K. or G.Y.Y.

Reprints and permissions information is available at www.nature.com/reprints.

Publisher's note Springer Nature remains neutral with regard to jurisdictional claims in published maps and institutional affiliations.

Open Access This article is licensed under a Creative Commons Attribution 4.0 International License, which permits use, sharing, adaptation, distribution and reproduction in any medium or format, as long as you give appropriate credit to the original author(s) and the source, provide a link to the Creative Commons licence, and indicate if changes were made. The images or other third party material in this article are included in the article's Creative Commons licence, unless indicated otherwise in a credit line to the material. If material is not included in the article's Creative Commons licence and your intended use is not permitted by statutory regulation or exceeds the permitted use, you will need to obtain permission directly from the copyright holder. To view a copy of this licence, visit http://creativecommons.org/licenses/by/4.0/.

© The Author(s) 2023